JMEPEG (2010) 19:852–859
DOI: 10.1007/s11665-009-9562-z

1059-9495/$19.00

The Effect of the Surface Treating and High-Temperature Aging on the Strength and SCC Susceptibility of 7075 Aluminum Alloy

Hamidreza Fooladfar, Babak Hashemi, and Mousa Younesi

(Submitted April 15, 2009; in revised form August 30, 2009)

A novel heat-treatment procedure combining the shot-peening with a two-step aging operation was proposed to improve both the strength and the stress corrosion cracking (SCC) resistance of the high-strength 7075 aluminium alloy. The heat treatment included one shot-peening stage before or between the two stages of aging at 120 °C for 24 h and at 160 °C for 1 h, respectively. The mechanical properties obtained during the aforementioned operations were extremely similar to those of the T6 sample owing to the unaffected bulk microstructure over such a low over-aging period. The SCC resistance of these samples was considerably improved compared to that of the T6 sample and of the conventional shot-peened T6 sample due to the over-aging of the surface like the T7 treatment leading from the diffusion acceleration by the dislocations generated in the surface layer during shot-peening. In spite of the further depth of deformation caused by shot-peening prior to the first step of aging, the sample shot-peened after the first step of aging showed no significant decrease in the SCC resistance because of its higher generated dislocation by shot-peening.

Keywords aerospace, aluminum, corrosion testing, heat treating, surface engineering

1. Introduction

The 7000-series aluminum alloys are widely used in aerospace industries due to their high strength and low density (Ref 1). The high strength of the 7000-series alloys is due to the fine and uniformly distributed precipitates which precipitate during the artificial aging in the matrix. The usual precipitation sequence of the 7000-series Al alloys can be summarized as (Ref 2):

Solid solution $\rightarrow$ GP zone $\rightarrow$ metastable $\acute{\eta}$ $\rightarrow$ stable η ($MgZn_2$)

The other structures along the transformation path are not so well known. For the peak aged (T6) 7000-series aluminium alloys, the $\acute{\eta}$ phase is the main precipitate; however, for the over-aged temper (T7×) the η phase is the main precipitate (Ref 3, 4). The stress corrosion cracking (SCC) resistance which reduces significantly after T6 heat treatment is of practical importance to the industrial applications of the 7000-series aluminium alloys. Many efforts have been made to correlate the heat treatment and the resultant microstructure with the SCC behavior of the alloys. The major microstructural features affecting the SCC resistance are the grain boundary precipitates (GBP). The SCC resistance can be improved by increasing both the size and the inter-particle distance of the GBP (Ref 5-7). It is known that the resistance of SCC can be improved to a great extent by over-aging, namely the T7× temper. Unfortunately, as compared with the T6 temper, the strength is reduced by 10 to 15 pct (Ref 8, 9). To satisfy the strength requirements for engineering applications, the size of the alloy parts must be enlarged. Therefore, it is essential to increase both the strength and the SCC resistance simultaneously in order to achieve more economical aircraft designs.

Therefore, extensive research efforts have been made to enhance both the strength and the SCC resistance of the 7000-series alloys. Cina (Ref 10) firstly proposed a heat treatment known as retrogression and reaging (RRA) on 7075 alloy to achieve that aim. The RRA included annealing of T6 sample at 180-240 °C for 5-2400 s (i.e., retrogression), which was followed by reaging using conditions similar to those used for the original T6 aging. After the RRA heat treatment, the precipitates on the grain boundaries of the alloys became coarse, whereas those within the grains were still fine. Thus, the SCC susceptibility of the alloys was reduced while the strength was kept similar to that obtained in conventional T6 sample. This treatment was only applicable for thin sections due to the short period of heating at retrogression. Ou et al. (Ref 4, 11) proposed a step-quench and aging (SQA) treatment for 7000-series alloys, in which the sample was quenched to a temperature of 200-220 °C from the solution-treatment temperature and was kept for 10-30 s, then was quenched to the room temperature and finally the quenched sample was aged to the T6 temper. This treatment improved the SCC resistance substantially due to the increased size and inter-particle distance of the GBP, while the strength of the sample was similar to that achieved in the T6 sample. Some of these

Hamidreza Fooladfar, Babak Hashemi, and **Mousa Younesi**, Department of Materials Science and Engineering, School of Engineering, Shiraz University, Shiraz, Iran. Contact e-mail: hamid_ff@yahoo.com.

treatments were studied in more detail and also were compared by Lin et al. (Ref 6). Huang et al. (Ref 12) and Song and Chen (Ref 13) proposed high-temperature pre-precipitating which cause grain boundary precipitate to enlarge and become discontinuous. However, these treatments were not suitable for the high quench sensitive 7000-series alloys such as Al-7075. Also, some other research was concentrated on obtaining bulk material with both high strength and low SCC susceptibility while just few ones have been attended to the surface treatments of these alloys despite the fact that the surface of the alloy has more severe responsibility in SCC initiation. However, the research was generally limited to explore different coatings or conventional shot-peening to avoid surface microcracks (Ref 14-16). In one case, it was reported that pre-immersion in an alkaline 3.5% NaCl for 240 h can be a contributor for enhancement in SCC resistance. This was attributed to the presence of copper oxide in the corrosion products (Ref 17).

A pre-strain is usually applied to the 7000-series alloys in the as-quenched state to relieve the quench-induced internal stress (Ref 18). It is well known that the dislocations generated in the pre-strain process can provide efficient sites for heterogeneous direct nucleation of the η precipitates and they are also fast diffusion paths for the precipitation elements in the aging process and can significantly influence the sequence of precipitation (Ref 19, 20).

Mechanical surface treatments such as shot-peening and ball-burnishing in addition to generating residual compressive stresses, which increases the resistance to fatigue crack nucleation (Ref 21, 22), can also induce a great amount of plastic deformation within the surface layer (Ref 23).

In this research, we have attempted to over-age simply the surface of Al-7075 alloy by grouping shot-peening as an effective mechanical surface treatment operation and age hardening in order to obtain a combination of both a high-strength bulk and a high-SCC-resistant surface.

2. Material and Procedures

The raw material used in this investigation was aluminum alloy (7075-T0), delivered in the form of a 6 mm thick plate of the chemical analysis illustrated in Table 1.

The samples were solution-treated at 470 °C for 2 h in a salt bath furnace and then were quenched into water at room temperature. Different treatment procedures as listed in Table 2 were performed after quenching. In addition to the traditional T6 and T73 treatments, a novel heat-treatment procedure which combined shot-peening and two-step aging signified as surface over aging (SOA) was proposed. SOA1 and SOA2 samples referred to the samples shot-peened before and between two steps of aging, respectively. As a comparison, a T6 heat-treated sample was subjected to conventional shot-peening with the same Almen intensity signified as T6SP. Shot-peening was done after sectioning the samples from the original sheet and preparing mini coupons for tensile test, in the unstressed condition using a gravity induction system with S280 cast steel shots. Peening was done at full cover-age to 0.30 mm A Almen intensity. In order to eliminate the induced distortion of the coupons after peening, the coupons were rolled with a roller gap equal to the original thickness of the coupons (0% reduction in area).

Table 1 The chemical compositions of 7075 Al alloy, wt.%

Zn	Mg	Cu	Fe	Si	Mn	Cr	Ti	Al
5.72	2.53	1.6	0.49	0.41	0.31	0.21	0.19	Balance

Dog-bone-shaped tensile samples with a gauge length of 25 mm and a gauge width of 6 mm and the as-finished thickness of the samples were machined with their axes parallel to rolling direction according to ASTM B557M specifications. The Vickers microhardness test was employed to determine the depth of penetration of the plastic deformation. The tensile properties were tested at a strain rate of 2×10^{-3} s^{-1} by using an Instron 8802 testing machine.

SCC resistance of the 7075 samples was evaluated using the slow strain rate test (SSRT) in the air and in a 3.5% NaCl aqueous solution with the gauge length of the samples being completely immersed during the test. Dog-bone-shaped samples with a gauge length of 10 mm, a width of 3 mm and a thickness of 2 mm were prepared from the plates with the tensile axes perpendicular to the rolling direction. Tensile tests were conducted at room temperature with a strain rate of 2×10^{-6} s^{-1} by using an Instron 5848 testing machine.

The fracture surfaces of the samples were observed by the scanning electron microscopy (SEM). The dislocation density was calculated from the grain size and microstrain obtained from XRD peak broadening (Ref 24, 25). XRD measurements were carried out on a Bruker, D8 advance x-ray diffractometer operated at 1.8 kW and equipped with a Cu target. θ-2θ scans from $2\theta = 10$ to 100° were performed to record the XRD pattern. The precipitates in the samples were analyzed by transmission electron microscopy (TEM). A HITACHI H90000-NA TEM with a high-resolution objective, which was operated under 360 kV, was used for this study. Thin foils for TEM were prepared by twin jet-polishing in 30% HNO_3, 70% ethanol solution cooled to −35 °C with liquid nitrogen at 19 V. Differential scanning calorimetry (DSC) experiments were performed on TAQ 1000. The heating rate was 10 K min^{-1}.

3. Results and Discussion

Figure 1 illustrates the tensile properties of the 7075 samples with various treatments. Both the yield strength (YS)

Table 2 Heat-treatment procedures used for 7075 Al alloy in this study

Temper	Heat treatment
T6	470 °C/2 h + water quench + 120 °C/24 h
T6SP	470 °C/2 h + water quench + 120 °C/24 h + shot peening
T73	470 °C/2 h + water quench + 120 °C/24 h + 160 °C/18 h
SOA1	470 °C/2 h + water quench + shot peening + 120 °C/24 h + 160 °C/1 h
SOA2	470 °C/2 h + water quench + 120 °C/24 h + shot peening + 160 °C/1 h

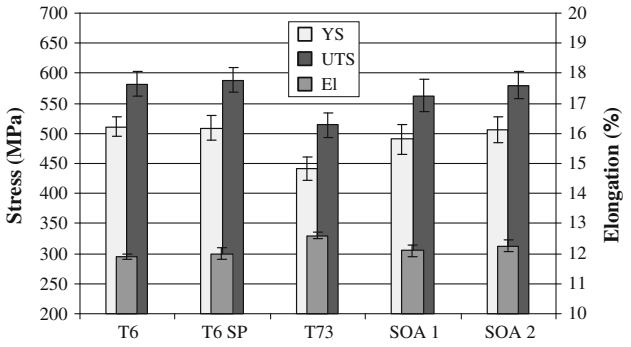

Fig. 1 Tensile properties of the 7075 samples with various heat treatments

Table 3 Transverse mechanical properties of differently treated 7075 samples at the strain rate of 2×10^{-6} s^{-1}

	UTS, MPa		Elongation, %		
Treatment	In air	In 3.5% NaCl	In air	In 3.5% NaCl	E_{sol}/E_{air} % (a)
T6	575	569	11.2	7.5	66.9
T6SP	583	573	11.3	8.8	77.8
T73	510	502	12	11.3	94.2
SOA1	557	551	11.4	9.9	86.8
SOA2	572	566	11.6	9.8	84.5

(a) E_{sol}/E_{air} = elongation tested in 3.5% NaCl/elongation tested in air

and ultimate tensile strength (UTS) of the T6 sample were higher than those of the T73 one. Similar results have been reported before (Ref 8). The T6SP sample exhibited higher UTS and El compared to the T6 sample due to the avoidance of the effect of the surface defects on premature failure. The mechanical properties of the two SOA samples were nearly the same as those of the T6 one. However, the strength of the SOA1 sample was slightly lower than that of the SOA2 sample; it was still higher than that of the T73 sample. It can be seen that by the SOA procedure, the mechanical properties expected of the T6 treatment can also be obtained to a considerable extent.

Table 3 shows the SSRT results of the differently treated samples in the air and in the 3.5% NaCl solution at a strain rate of 2×10^{-6} s^{-1}. Since these samples were tested perpendicular to the rolling direction at a lower strain rate, the UTS values of the samples tested in the air were slightly lower than those shown in Fig. 1. The UTS values of the samples tested in the 3.5% NaCl solution were similar to those tested in the air. However, the elongations in the 3.5% NaCl solution were lower than those in the air. In this study, we used an index E_{sol}/E_{air} to evaluate the SCC resistance, which is the ratio of the elongations of the samples tested in the 3.5% NaCl solution and in the air (shown in Table 3). The greater the E_{sol}/E_{air} value is, the higher the SCC resistance is. The E_{sol}/E_{air} value of 1 implies that the material exhibits no SCC susceptibility. The lowest E_{sol}/E_{air} value observed in the T6 sample indicates that the T6 sample had the lowest SCC resistance among these samples. Similar results were also reported in the other 7000-aluminum alloys (Ref 26). The E_{sol}/E_{air} of the T6SP sample, as expected, was higher than that of the T6 sample owing to its surface compressive residual stress induced by shot-peening. In the SOA samples, the E_{sol}/E_{air} was much closer to that of the T73 sample, implying that in comparison with the conventional shot-peened T6 sample, the SOA samples were more comparable to the T73 sample in terms of SCC resistance, indicating that the SOA procedure can improve the SCC resistance of the alloy more effectively. Nonetheless, the SCC susceptibility of the SOA1 sample was slightly lower than that of the SOA2 sample.

Figure 2 presents the typical tensile fracture surfaces of the T6, T73, SOA1 and SOA2 samples tested in the aqueous chloride solutions. The fracture surface of the T6 sample was dominated by the intergranular fracture with severe corrosion, showing a great deal of the brittle fracture and SCC attack (Fig. 2a). In contrast, intergranular microvoid coalescences were found in the T73 sample (Fig. 2b). This is attributed to the preferential deformation of the precipitate-free zone around the grain boundary area (Ref 25). Furthermore, a number of large dimples and cleavage facets were also observed on the fracture surface of this sample. The bulk of both the SOA samples (Fig. 2c, e) shows the same fracture surface as that of the T6 sample, representing that the bulk of the sample was not influenced by the SOA procedure.

In the fractography image of the surface of the SOA samples, the dimples nearly disappeared and the fracture surface was characterized by the intergranular microvoid coalescences and cleavage facets which were very similar to that in the T73 sample (Fig. 2d, f). The predominance of the intergranular fracture suggested that the grain boundaries were the preferential paths for the SCC.

Figure 3 shows the grain boundary precipitates in the 7075 samples with various treatments. Regarding the SOA samples, the TEM images of the surface and the bulk are shown individually. The precipitates on the grain boundaries of the T6 sample were small and distributed continuously (Fig. 3a) but in the T73 sample the grain boundaries were decorated with the coarse and discontinuously distributed particles (Fig. 3b). This is similar to the previous reports (Ref 5, 11). The grain precipitates and grain boundary precipitates in the bulk of the SOA1 and SOA2 samples (Fig. 3c, e) were extremely similar to those of the T6 sample (Fig. 3a), confirming that the microstructure of the bulk was unaffected during the SOA operation. The quantitative similarity of the yield strength and UTS of the SOA samples to the T6 ones is due to the fact that the bulk strength of a sample represents the total strength of the sample, regardless of the surface strength.

On the other hand, the surface grains in the SOA1 and SOA2 samples (Fig. 3d, f) were filled with the high density of dislocations, created during shot-peening. The existence of more precipitates on the dislocation and their surroundings indicated that the precipitates were preferentially formed on dislocation networks as heterogeneous sites rather than dislocation-free zones. Moreover, the grain boundary precipitates of the surfaces of the SOA samples were considerably larger than those in the T6 sample (Fig. 3a) and their inter-particle distance was also larger than that in the T6 sample. This configuration was more evident in the SOA1 sample. Furthermore, precipitates within the grain of the SOA1 sample were larger and more heterogeneous than those in the SOA2 sample. For the 7000-series alloys, the pre-strain usually resulted in the generation of the equilibrium phase η ($MgZn_2$) on the dislocation network; therefore, it reduced the amount of

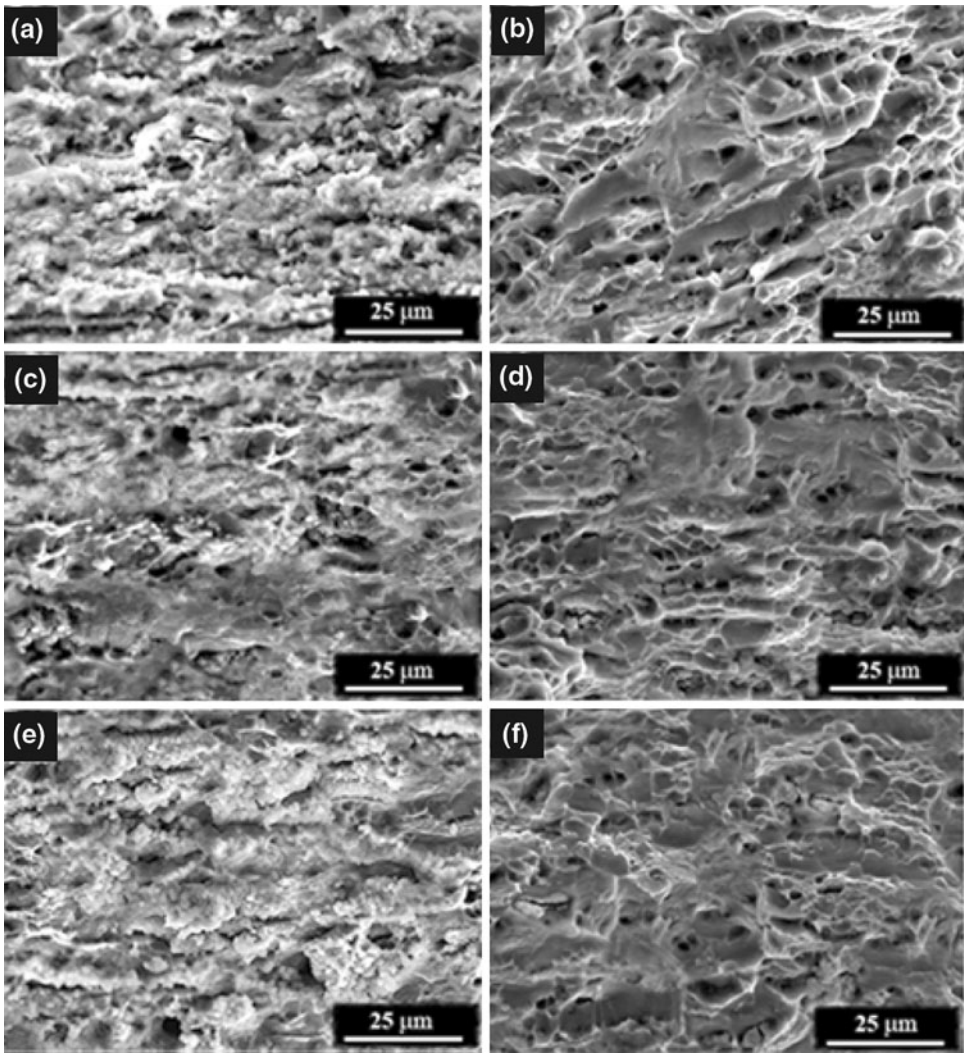

Fig. 2 SEM micrographs showing SSRT fracture surfaces of differently treated 7075 samples in 3.5% NaCl solution: (a) T6, (b) T73, (c) SOA1 bulk, (d) SOA1 surface, (e) SOA2 bulk, and (f) SOA2 surface

the solutes for the formation of the main hardening phase ή in the T6 sample, leading to decrease in the mechanical strength of the alloys (Ref 19, 27). In the SOA1 sample, the η phase pre-nucleated on the grain boundaries. At the same time, some dislocations produced by the pre-strain treatment were aggregated around the grain boundaries. Wang and Ma (Ref 28) have reported that similar to the situation in the grains, the dislocations in the grain boundaries also provide heterogeneous nucleation sites for the η phase particles. Both the modes contributed to the nucleation of the η phase on the grain boundaries and the η phase grew in the subsequent aging at 160 °C, which made the grain boundary precipitates enlarge and distribute discontinuously. On the other hand, similar to the GBPs, the precipitates nucleated on the dislocations within the grains enlarged, causing the strength to diminish.

The SOA1 sample had larger grain boundary precipitates and longer inter-particle distance but the size was still smaller than that in the T73 sample. The small and discontinuously distributed grain boundary particles are considered to be beneficial to the toughness of the samples (Ref 29). A slight increase in the elongation of the SOA2 sample compared to the SOA1 sample was observed (Table 3).

Concerning the 7000-series aluminum alloys, the stress corrosion cracking resistance was related to the grain boundary precipitates. The mechanism of the SCC in the Al-Zn-Mg-Cu alloys was considered to be both anodic dissolution and hydrogen embrittlement (Ref 30). The precipitates in the grain boundaries are Mg-rich phases in these alloys, which have the electrode potential different from the Al matrix (Ref 31). This resulted in the anodic dissolution and formed critical defects at the first stage of the SCC process in the aqueous chloride solutions. Furthermore, the hydrogen produced in the crack tip also leads to the hydrogen embrittlement in the grain boundaries. However, the lattice diffusion coefficients of hydrogen in the FCC materials such as the aluminum alloys are very low. This means that there should be a number of more rapid transport modes for hydrogen. It is well known that grain boundary is one of the rapid diffusion paths in a material, which accelerated the hydrogen transport. Moreover, Albrecht et al. (Ref 32) examined another possible mode and suggested that the mobile dislocations generated in the tip of the crack improve the hydrogen diffusion in the matrix. Neguyen et al. (Ref 33) proposed that the increment of the precipitate size and the associated change from the GP zone to the semicoherent ή

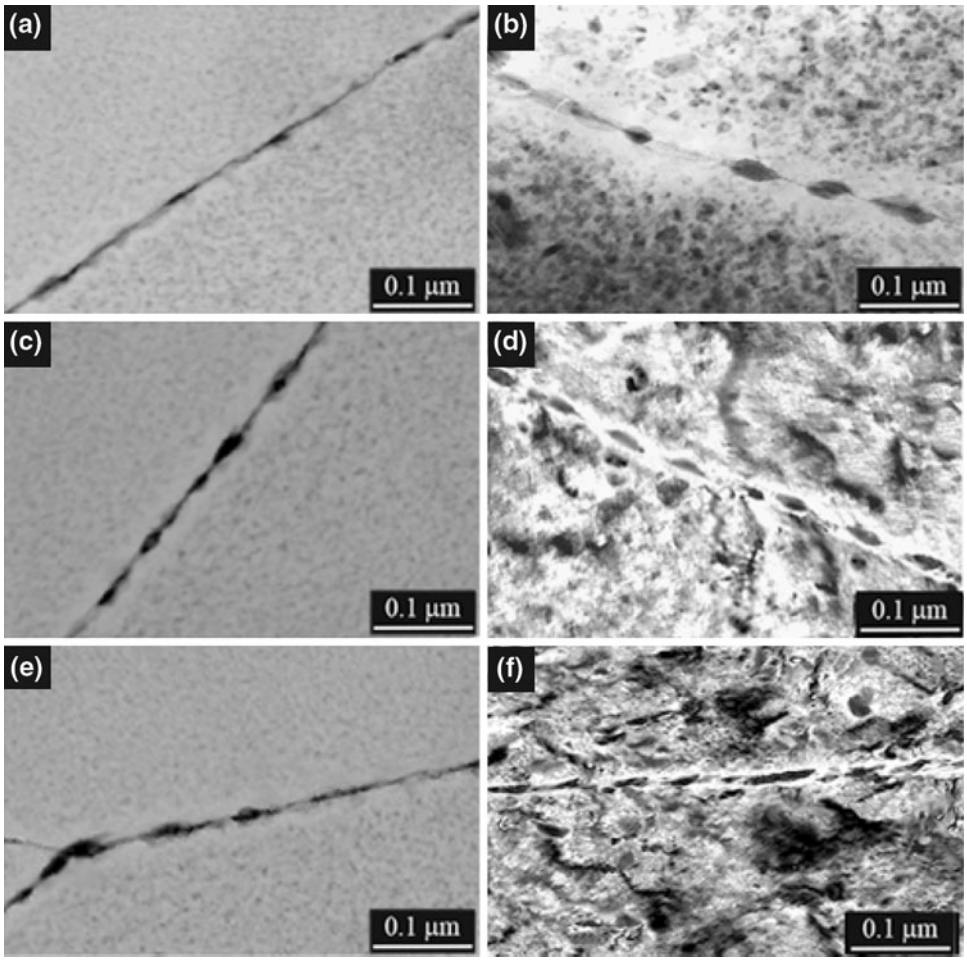

Fig. 3 TEM micrographs showing grain boundary precipitates of 7075 samples: (a) T6, (b) T73, (c) SOA1 bulk, (d) SOA1 surface, (e) SOA2 bulk, and (f) SOA2 surface

and incoherent η precipitates result in a more homogeneous slip mode and a reduction in slip planarity. This could effectively decrease the mobile dislocation and, in a larger amount, reduce the hydrogen transported to the grain boundaries in the SOA samples. Therefore, more homogeneous slip mode appeared in the SCC process in order to inhibit the hydrogen diffusion. Due to the fact that the stress corrosion cracks initiate from the surface, the SOA samples had higher SCC resistance compared to the T6 sample. In addition, Song et al. (Ref 34, 35) reported that the element Mg in the grain boundaries had a larger electronegativity difference between Mg and H atoms than that between Al and H atoms. Therefore, the element Mg in the grain boundaries could increase the amount of hydrogen absorbed and consequently accelerate its diffusion and enhance the solution degree of hydrogen in the grain boundaries. This resulted in the embrittlement of the grain boundaries and accelerated the growth of the stress corrosion cracks. The large size and inter-particle spacing of the surface grain boundary particles could decrease the anodic dissolution speed and act as the trapping sites for atomic hydrogen and create molecular hydrogen bubbles to reduce the concentration of the atomic hydrogen in the grain boundaries. Both the size and the inter-particle distance of the grain boundary precipitates in the SOA samples and the T73 sample were larger than those in the T6 sample. Therefore, the SCC resistance of these samples was significantly higher than that of the T6 sample.

The calorimetric curves after solution-treatment and shot-peening for the bulk and surface samples are presented in Fig. 4; peak temperatures representing the maximum reaction rate temperature and enthalpy can be measured by the area under the peak, proportional to the volume fraction of the precipitate undergoing dissolution or formation. The bulk calorimetric curve shows four exothermic peaks corresponding to several precipitation reactions, and a broad endothermic peak, at high temperature corresponding to a dissolution reaction. According to the sequence of precipitating in the 7000-series of Al alloys, the first peak observed must then correspond to GP zones formation; the second to ή; and the third to η; whilst the fourth exothermic peak, according to Deiasi and Adler (Ref 36), is a consequence of the η growth by Ostwald ripening; and the final endothermic peak is the result of η dissolution. The location and intensity of the peaks in the surface curve are remarkably different from those of the bulk sample. The first exothermic peak attributed to the GP zone is quite eliminated in the surface curve. Furthermore, the peak of the formation of ή nearly coalesced to the peak of forming η, which occurred at a lower temperature as well as with higher intensity, indicating the great effect of dislocations generated by shot-peening on the sequence of precipitation. The premature

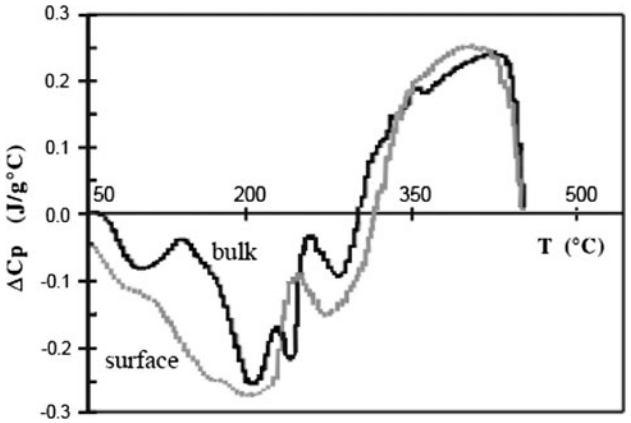

Fig. 4 Calorimetric curves of Al-7075 after solution-treatment, quenching and post shot-peening for the bulk and for the surface of the sample

formation of η phase with higher intensity allows for the over-aging of the sample over a considerably shorter period of time. As a result, the surfaces of the shot-peened samples were over-aged during the short time of the second stage of aging while keeping the bulk unaffected.

Figure 5(a) illustrates the microhardness of the solution-treated and the T6 samples versus distance from the surface after the shot-peening process. Both samples showed the enhanced surface hardness which was decreased by increasing the distance from the surface. However, this decrease was more severe in the solution-treated sample, whereas the surface hardness of the solution-treated sample was lower than that of the T6 one as well. This can be related to the higher capability of the solutionized sample to strain hardening during shot-peening. This is due to its superior work hardenability as expected (Ref 37). The depth of the deformation caused by shot-peening was higher for the solutionized sample due to its lower strength. Furthermore, the higher primary hardness of the T6 sample owing to age hardening causes its higher surface hardness. Moreover, the microhardness of both the samples had a reverse mode after the second stage of aging (Fig. 5b). With the same condition for both of the samples, the surfaces showed the lowest hardness which increased to reach the maximum hardness obtained from T6 treatment and remained constant for deeper regions. Comparing Fig. 5(a) and (b) reveals that the depth of over-aging was the same as the depth of deformation caused by shot-peening, meaning that this deformation was the main reason for surface over-aging. The correlation between the depth of the deformation and depth of over-aging led to the deeper surface over-aging of the SOA1 sample, resulting in the lower strength and SCC susceptibility of this sample.

The average grain size D and microstrain was calculated from the XRD peak broadening (Ref 25), dislocations density ρ can be represented in terms of the grain size D and microstrain $\langle \varepsilon^2 \rangle^{1/2}$ by (Ref 24, 38):

$$\rho = 2\sqrt{3}\langle \varepsilon^2 \rangle^{1/2}/(D * b) \qquad \text{(Eq 1)}$$

where b is the Burgers vector which is equal to $\sqrt{2}a/2$ for an fcc Al alloy. The calculated ρ after shot-peening from the surface on the way to the undeformed metal for the solutionized and T6 samples is shown in Fig. 6. The surface dislocation density of both samples has been greatly amplified due

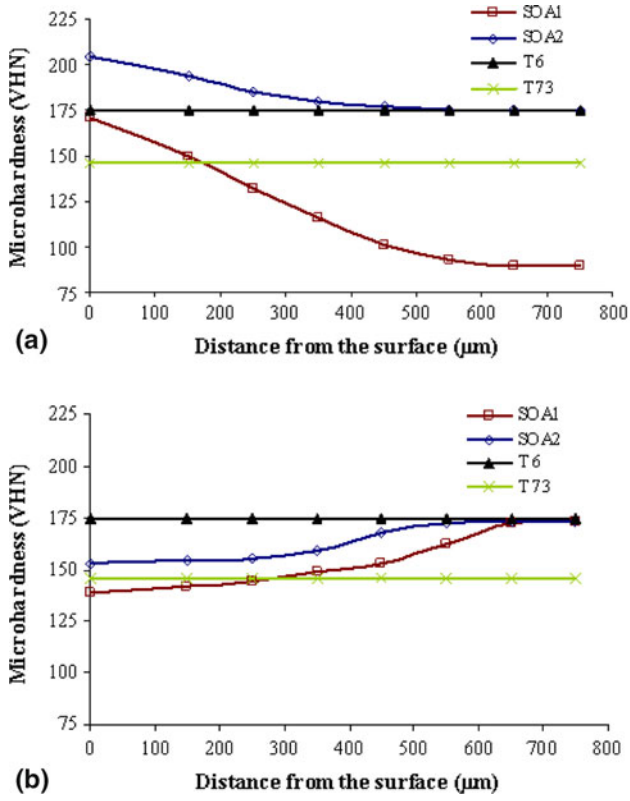

Fig. 5 Microhardness-depth profile of the SOA1 and SOA2 samples: (a) after the shot-peening and (b) after the second stage of aging

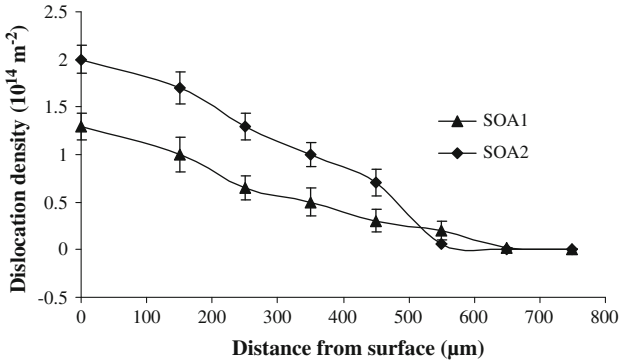

Fig. 6 The calculated dislocation density after shot-peening and before the last aging for the SOA1 and the SOA2 samples

to the high surface plastic deformation induced during shot-peening but this amount decreased by increasing the distance from the surface as a result of the lack of deformation and consequently at a definite depth reached a neglectable quantity compared with the surface dislocation density. It can be seen that ρ of the T6 sample has been higher than that of the solutionized one in the entire depth of deformed zone to 520 μm where it corresponded to the last severely deformed region by shot-peening. The secondary phase particles in the T6 sample played a critical and positive role in dislocation generation during shot-peening (Ref 39) and increased the density of the generated dislocations. Increasing the density

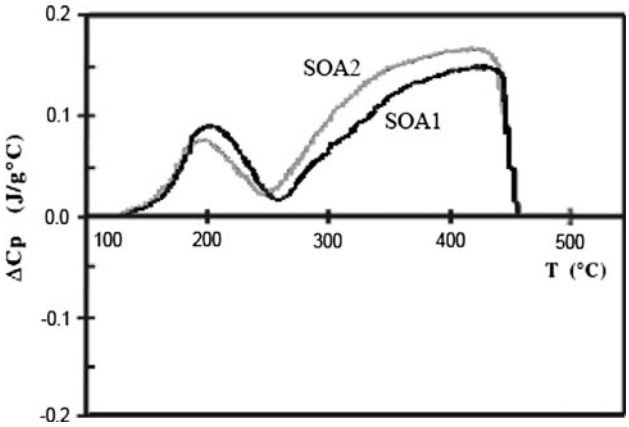

Fig. 7 Calorimetric curves of the surface of the 7075 alloy after the SOA1 and the SOA2 treatments

of dislocations can accelerate the dissolution of the metastable GP zones and ή particles and creates more stable η phase. This ultimately reduces the SCC susceptibility of the surface layer (Ref 40).

The calorimetric curves of the surfaces of SOA1 and SOA2 samples, illustrated in Fig. 7, show two endothermic reactions in both the samples; the low-temperature peak resulting from the ή dissolution process and the high-temperature peak from the η dissolution reaction. In the DSC curve of the SOA2 sample, both peaks occur at slightly lower temperatures than those of the SOA1 sample as a result of containing higher density of dislocations. Furthermore, in comparison with the SOA1 curve, the SOA2 curve has a lower area under the first peak, while it has a bigger area under the second peak. These results revealed well that the SOA2 sample had a higher amount of η phase precipitates as compared with the SOA1 sample, confirming that the transformation of ή to η was more complete in this sample. These results are in agreement with the TEM microstructural characterization. Therefore, the shot-peening between the two stages of aging was more effective in achieving the entire surface over-aged end product than doing it before the two stages of aging. This effect is contrary to the effect of the reduction in the GBP size caused by the high density of dislocations and leads to the achievement of the SCC resistance more than expected. Hence, this has no disagreement with the results obtained by Wang and Ma (Ref 28).

4. Conclusion

1. The dislocations created during shot-peening could effectively change the sequence of precipitation and enhanced the rate of the precipitation of the η phase at subsequent aging. Therefore, the created dislocations allowed for the over-aging of the surface without influencing the bulk of the sample.
2. Both of the SOA samples had lower SCC susceptibility than the conventional shot-peened T6 sample, indicating that the surface over-aging could improve the SCC resistance more efficiently.
3. Shot-peening before the first stage of aging caused further depth of deformation than between the two stages of aging due to the lower strength of the solutionized sample. The reason for the higher SCC resistance of the SOA1 sample was more depth of over-aging and the larger size and inter-particle space of the grain boundary precipitates in this sample than the SOA2 sample. On the other hand, these characterizations led to the sacrifice of the SOA1 sample strength to some extent.
4. Precipitates formed at the first stage of the aging function as a dislocation generating source, resulting in an increase in dislocation generation during shot-peening in the SOA2 sample. This consequently led to more completely over-age of the surface. Therefore, despite the other effect of higher dislocation density of the SOA2 sample which caused smaller and more continued GBPs, it had no considerable SCC resistance weakening as compared with the SOA1 sample.
5. Since over-aging was simply limited to the surface of the SOA samples, their strength was considerably similar to that of the T6 sample; nonetheless, the strength loss of the SOA1 sample was more obvious.

Acknowledgments

The financial support for this research (grant number 86-GR-ENG-62) given to Dr. B. Hashemi by the Research Committee of Shiraz University is gratefully appreciated.

References

1. J.E. Hatch, Ed., *Aluminum Properties and Physical Metallurgy*, American Society for Metals, OH, 1984
2. G. Sha and A. Cerezo, Early-Stage Precipitation in Al–Zn–Mg–Cu Alloy (7050), *Acta Mater.*, 2004, **52**, p 4503
3. N.Q. Chinh, J. Lendvai, D.H. Ping, and K. Hono, The Effect of Cu on Mechanical and Precipitation Properties of Al–Zn–Mg Alloys, *J. Alloys Compd.*, 2004, **378**, p 52
4. B.L. Ou, J.G. Yang, and M.Y. Wei, Effect of Homogenization and Aging Treatment on Mechanical Properties and Stress-Corrosion Cracking of 7050 Alloys, *Metall. Mater. Trans.*, 2007, **38A**, p 1760
5. M. Puiggali, A. Zielinski, J.M. Olive, E. Renauld, D. Desjardins, and M. Cid, Effect of Microstructure on Stress Corrosion Cracking of an Al-Zn-Mg-Cu Alloy, *Corros. Sci.*, 1998, **40**, p 805
6. J.C. Lin, H.L. Liao, W.D. Jehng, C.H. Chang, and S.L. Lee, Effect of Heat Treatments on the Tensile Strength and SCC-Resistance of AA7050 in an Alkaline Saline Solution, *Corros. Sci.*, 2006, **48**, p 3139
7. K. Rajan, W. Wallace, and J.C. Beddoes, Microstructural Study of a High-Strength Stress-Corrosion Resistant 7075 Aluminium Alloy, *J. Mater. Sci.*, 1982, **17**, p 2817
8. A.F. Oliveira, M.C. de Barros, K.R. Cardoso, and D.N. Travessa, The Effect of RRA on the Strength and SCC Resistance on AA7050 and AA7150 Aluminium Alloys, *Mater. Sci. Eng. A*, 2004, **379**, p 321
9. M. Dixit, R.S. Mishra, and K.K. Sankaran, Structure–Property Correlations in Al 7050 and Al 7055 High-Strength Aluminum Alloys, *Mater. Sci. Eng. A*, 2008, **478**, p 163
10. B.M. Cina, Reducing the Susceptibility of Alloys, Particularly Aluminum Alloys, to Stress Corrosion Cracking, U.S. Patent 3,856,584, 1974
11. B.L. Ou, J.G. Yang, and C.K. Yang, Effects of Step-Quench and Aging on Mechanical Properties and Resistance to Stress Corrosion Cracking of 7050 Aluminum Alloy, *Mater. Trans.*, 2000, **41**, p 783
12. L.P. Huang, K.H. Chen, S. Li, and M. Song, Influence of High-Temperature Pre-Precipitation on Local Corrosion Behaviors of Al–Zn–Mg Alloy, *Scr. Mater.*, 2007, **56**, p 305
13. M. Song and K. Chen, Effects of the Enhanced Heat Treatment on the Mechanical Properties and Stress Corrosion Behavior of an Al–Zn–Mg Alloy, *J. Mater. Sci.*, 2008, **43**, p 5265

14. S. You, P. Jones, A. Padwal, P. Yu, M. O'Keefe, W. Fahrenholtz, and T. O'Keefe, Response of Nanocrystalline Cerium-Based Conversion Coatings on Al 2024–T3 to Chloride Environments, *Mater. Lett*, 2007, **61**(17), p 3778
15. H. Rahmatalla, M. Al-Rimawi, and T. Al-Hadid, Effect of Shot-Peening on Stress Corrosion Cracking (SCC) of 7075-T6 Aluminium Alloy, *Proceedings of the ICSP-6 Conference*, 1996, p 184
16. J. Fader, C. Keeney, J. Hawkins, M. Clements, and S. Yollick, Anti-Corrosion Coating Applied During Shot-Peening Process, U.S. Patent 6,874,214, 2005
17. H.L. Liao, J.C. Lin, and S.L. Lee, Effect of Pre-Immersion on the SCC of Heat-Treated AA7050 in an Alkaline 3.5% NaCl, *Corros. Sci.*, 2009, **51**, p 209
18. A. Deschamps, Y. Brechet, P. Guyot, and F. Livet, On the Influence of Dislocations on Precipitation in an Al-Zn-Mg Alloy, *Z. Metallkd.*, 1997, **88**, p 601
19. A. Deschamps, F. Livet, and Y. Brechet, Influence of Predeformation on Ageing in an Al–Zn–Mg Alloy—I. Microstructure Evolution and Mechanical Properties, *Acta Mater.*, 1999, **47**, p 281
20. M. Talianker and B. Cina, Retrogression and Reaging and the Role of Dislocations in the Stress Corrosion of 7000-Type Aluminum Alloys, *Metall. Trans.*, 1989, **20A**, p 2087
21. L. Wagner and C. Mueller, Effect of Shot-Peening on Fatigue Behaviour in Al-Alloys, *Mater. Manuf. Processes*, 1992, **7**, p 423
22. M. Hilpert, ''Dauerschwingverhalten von Magnesiumlegierungen: Einfluss von mechanischen Oberflächenbehandlungen und Umgebungsmedien,'' Dr.-Ing. Thesis, BTU Cottbus, 2001
23. J.K. Gregory and L. Wagner, *Shot-Peening*, L. Wagner, Ed., Wiley–VCH, Weinheim, 2003
24. Y.H. Zhao, X.Z. Liao, Z. Jin, R.Z. Valiev, and Y.T. Zhu, Microstructures and Mechanical Properties of Ultrafine Grained 7075 Al Alloy Processed by ECAP and Their Evolutions During Annealing, *Acta Mater.*, 2004, **52**, p 4589
25. Y.H. Zhao, K. Zhang, and K. Lu, Structure Characteristics of Nanocrystalline Element Selenium with Different Grain Sizes, *Phys. Rev. B*, 1997, **56**, p 14322
26. T.C. Tsai, J.C. Chang, and T.H. Chuang, Stress Corrosion Cracking of Superplastically Formed 7475 Aluminum Alloy, *Metall. Mater. Trans.*, 1997, **28A**, p 2113
27. G. Waterloo, V. Hansen, J. Gjonnes, and S.R. Skjervold, Effect of Predeformation and Preaging at Room Temperature in Al–Zn–Mg–(Cu, Zr) Alloys, *Mater. Sci. Eng. A*, 2001, **303**, p 226
28. D. Wang and Z.Y. Ma, Effect of Pre-strain on Microstructure and Stress Corrosion Cracking of Over-Aged 7050 Aluminum Alloy, *J. Alloys Compd.*, 2009, **469**, p 445
29. D. Dumont, A. Deschamps, and Y. Brechet, On the Relationship Between Microstructure, Strength and Toughness in AA7050 Aluminum Alloy, *Mater. Sci. Eng. A*, 2003, **356**, p 326
30. D. Najjar, T. Magnin, and T.J. Warner, Influence of Critical Surface Defects and Localized Competition Between Anodic Dissolution and Hydrogen Effects During Stress Corrosion Cracking of a 7050 Aluminium Alloy, *Mater Sci. Eng. A*, 1997, **238**, p 293
31. *Metals Handbook*, Vol 1, American Society for Metals, Cleveland, OH, 1961
32. J. Albrecht, I.M. Bernstein, and A.W. Thompson, Evidence for Dislocation Transport of Hydrogen in Aluminum, *Metall. Trans.*, 1982, **13A**, p 811
33. D. Nguyen, A.W. Thompson, and I.M. Bernstein, Microstructural Effects on Hydrogen Embrittlement in a High Purity 7075 Aluminum Alloy, *Acta Metall.*, 1987, **35**, p 2417
34. R.G. Song, W. Dietzel, B.J. Zhang, W.J. Liu, M.K. Tseng, and A. Atrens, Stress Corrosion Cracking and Hydrogen Embrittlement of an Al–Zn–Mg–Cu Alloy, *Acta Mater.*, 2004, **52**, p 4727
35. R.G. Song, M.K. Tseng, B.J. Zhang, J. Liu, Z.H. Jin, and K.S. Shin, Grain Boundary Segregation and Hydrogen-Induced Fracture in 7050 Aluminium Alloy, *Acta Mater.*, 1996, **44**, p 3241
36. R. Deiasi and P.N. Adler, Calorimetric Studies of 7000 Series Aluminum Alloys: I. Matrix Precipitate Characterization of 7075, *Metall Trans.*, 1977, **8A**, p 1177
37. Y.H. Zhao, X.Z. Liao, S. Cheng, E. Ma, and Y.T. Zhu, Simultaneously Increasing the Ductility and Strength of Nanostructured Alloys, *Adv. Mater.*, 2006, **18**, p 2280
38. R.E. Smallman and K.H. Westmacott, Stacking Faults in Face-Centred Cubic Metals and Alloys, *Philos. Mag.*, 1957, **2**, p 669
39. S. Cheng, Y.H. Zhao, Y.T. Zhu, and E. Ma, Optimizing the Strength and Ductility of Fine Structured 2024 Al Alloy by Nano-Precipitation, *Acta Mater.*, 2007, **55**, p 5822
40. I.J. Polmear, *Light Alloys*, 4th ed., Butterworth-Heinmann, Oxford, 2006